

Supporting information

Modulation Mechanism of Ionic Transport through Short Nanopores by Charged Exterior Surfaces †

Long Ma,^{a,b} Zhe Liu,^a Jia Man,^a Jianyong Li,^a Zuzanna

S. Siwy^c and Yinghua Qiu^{a,b,d*}

a. Key Laboratory of High Efficiency and Clean Mechanical Manufacture of Ministry of Education, National Demonstration Center for Experimental Mechanical Engineering Education, School of Mechanical Engineering, Shandong University, Jinan, 250061, China

b. Shenzhen Research Institute of Shandong University, Shenzhen, 518000, China

c. Department of Physics and Astronomy, University of California, Irvine, California 92697, United States

d. Suzhou Research Institute of Shandong University, Suzhou, 215123, China

†. Electronic supplementary information (ESI) available. See electronic supplementary information for simulation details, additional simulation results of ionic current through nanopores, and ion concentration distributions inside nanopores.

*Corresponding author: yinghua.qiu@sdu.edu.cn

1. Simulation details

In this part, simulation details are provided. The schematic illustration of simulations is shown in S1. The boundary conditions used in the simulations are listed in Table S1. Figure S2 shows the protocol for mesh building.

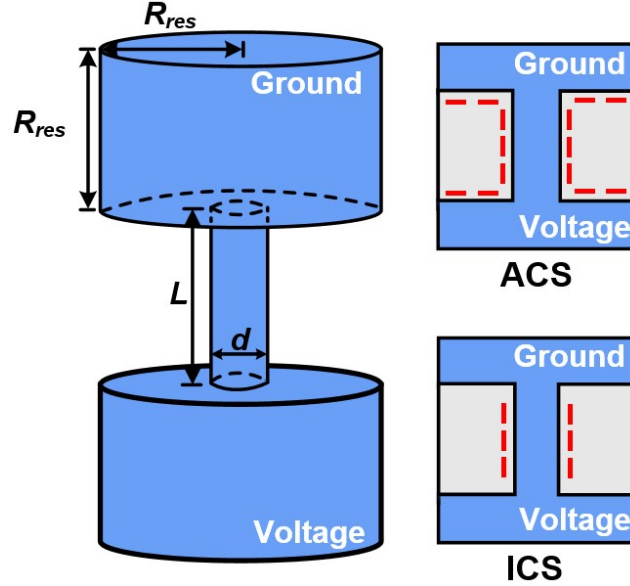
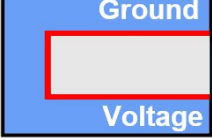
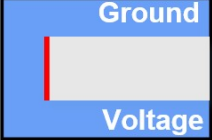


Figure S1 Schematic illustration of simulations. Negatively charged surfaces are shown with red dashed lines.

Table S1. Boundary conditions used in numerical modeling. Coupled Poisson-Nernst-Planck and Navier-Stokes equations were solved with COMSOL Multiphysics 5.2 package.

Scheme	Surface	Poisson	Nernst-Planck	Navier-Stokes
	AB	constant potential (Ground) $\phi=0$	constant concentration $c_i=C_{bulk}$	constant pressure $p=0$ no viscous stress $\mathbf{n} \cdot [\mu(\nabla \mathbf{u} + (\nabla \mathbf{u})^T)] = 0$
	BC, FG	no charge $-\mathbf{n} \cdot (\epsilon \nabla \phi) = 0$	no flux $\mathbf{n} \cdot \mathbf{N}_i = 0$	no slip
	HG	constant potential $\phi=V_{app}$	constant concentration $c_i=C_{bulk}$	constant pressure $p=0$ no viscous stress $\mathbf{n} \cdot [\mu(\nabla \mathbf{u} + (\nabla \mathbf{u})^T)] = 0$
	AH	axial symmetry	axial symmetry	axial symmetry

 <p>ACS</p>	CD, DE, EF	$-\mathbf{n} \cdot (\epsilon \nabla \phi) = \sigma_w$	no flux $\mathbf{n} \cdot \mathbf{N}_i = 0$	no slip $\mathbf{u} = 0$
 <p>ICS</p>	DE	$-\mathbf{n} \cdot (\epsilon \nabla \phi) = \sigma_w$	no flux $\mathbf{n} \cdot \mathbf{N}_i = 0$	no slip $\mathbf{u} = 0$
	CD, EF	no charge $-\mathbf{n} \cdot (\epsilon \nabla \phi) = 0$		

ϕ , ϵ , C_L , C_H , p , \mathbf{n} , \mathbf{N}_i , \mathbf{u} , σ_w , μ are the surface potential, dielectric constant, low bulk concentration, high bulk concentration, pressure, normal vector, flux of ions, fluid velocity, surface charge density of the pore wall, solution viscosity, respectively.

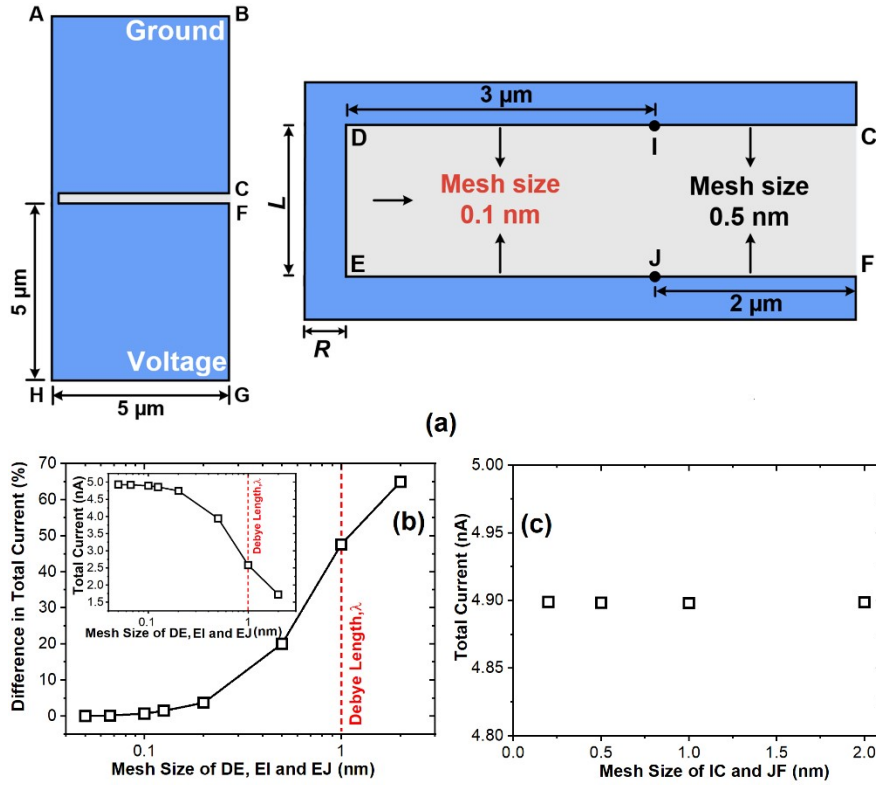


Figure S2. (a) Scheme of built mesh in simulations. For the inner pore surface (DE) and 3 μm-wide regions of exterior surfaces beyond the pore boundary (DI and EJ), the mesh size of 0.1 nm was used. For the rest part of exterior surfaces (IC and JF), a 0.5 nm mesh size was chosen. (b-c) The convergence of ionic current through the nanopore with different mesh sizes. (b) Different mesh sizes on surfaces of DE, EI, and EJ. The inset shows the total current as a function of the mesh size of DE, EI, and EJ. For the case with the mesh size of 0.05 nm, the obtained ionic current is used as the reference. The other points were calculated by the current difference over the reference current. (c) Different mesh sizes on surfaces of IC and JF.

Table S2. Thickness of EDLs in differently concentrated solutions

Concentration (mM)	Thickness of EDLs (nm)
10	3.04
30	1.76
50	1.36
100	0.96
200	0.68
300	0.56
400	0.45
500	0.43

2. Supported simulation results

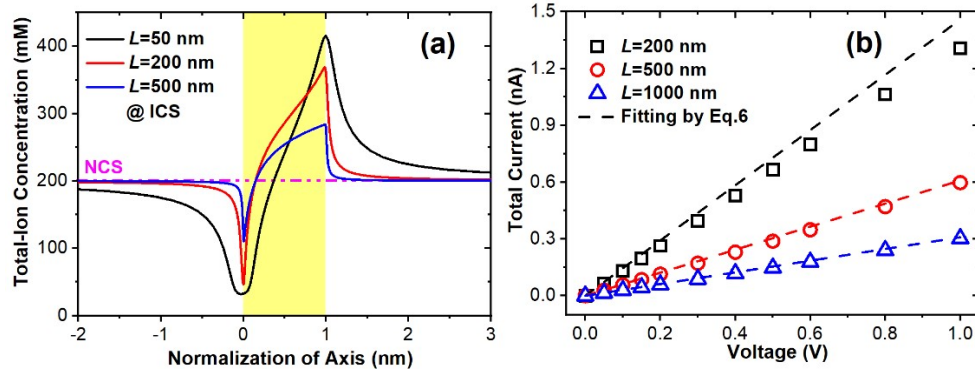


Figure S3. Concentration distributions of total ions along the pore axis (a), and IV curves of the ICS case at different pore lengths (b).

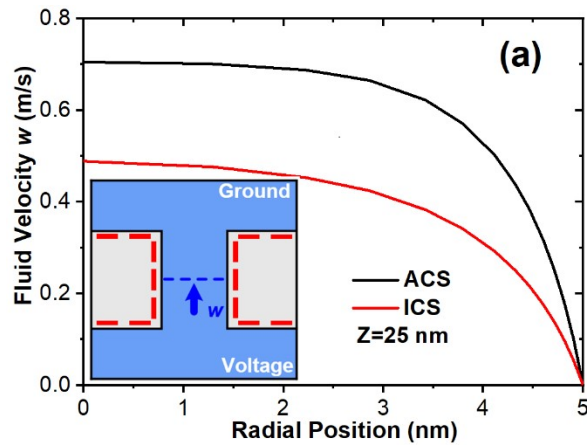


Figure S4. Radial distributions of fluid velocity (axial component w) in the center cross-section of the nanopores.

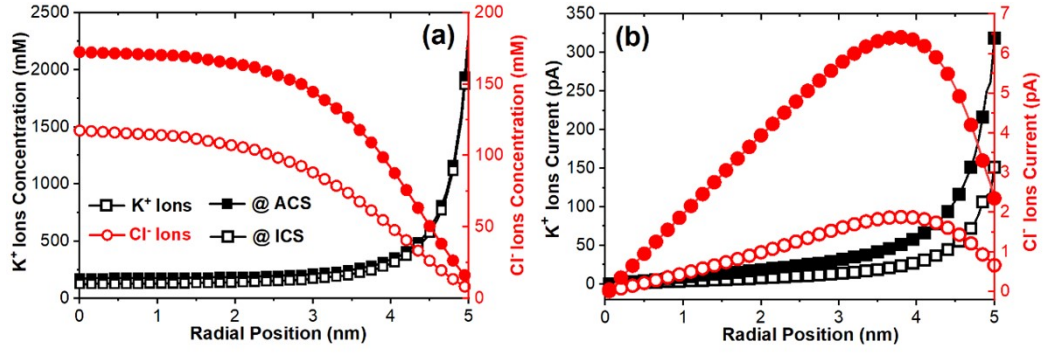


Figure S5. Distributions of ion concentration (a) and ionic current (b) in the center cross-section of the nanopores in the ACS and ICS cases. Each point of ion current density was obtained through the integration of ionic flux over 0.05-nm-wide segments.

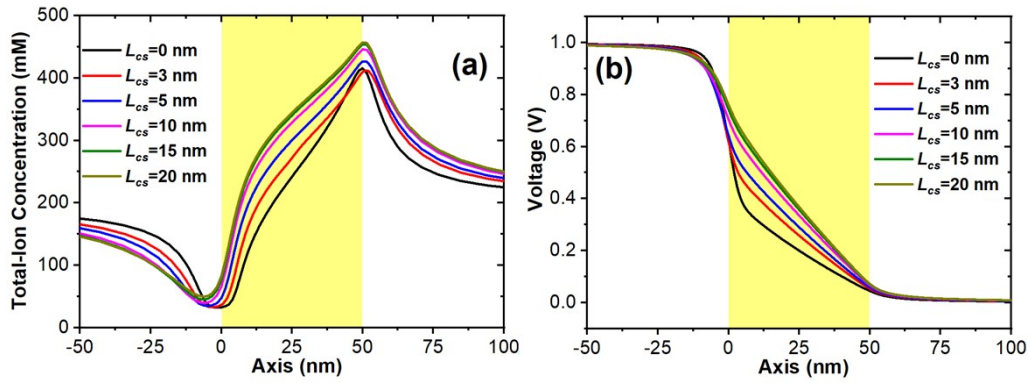


Figure S6 Axial distributions of ion concentration (a), potential (b).

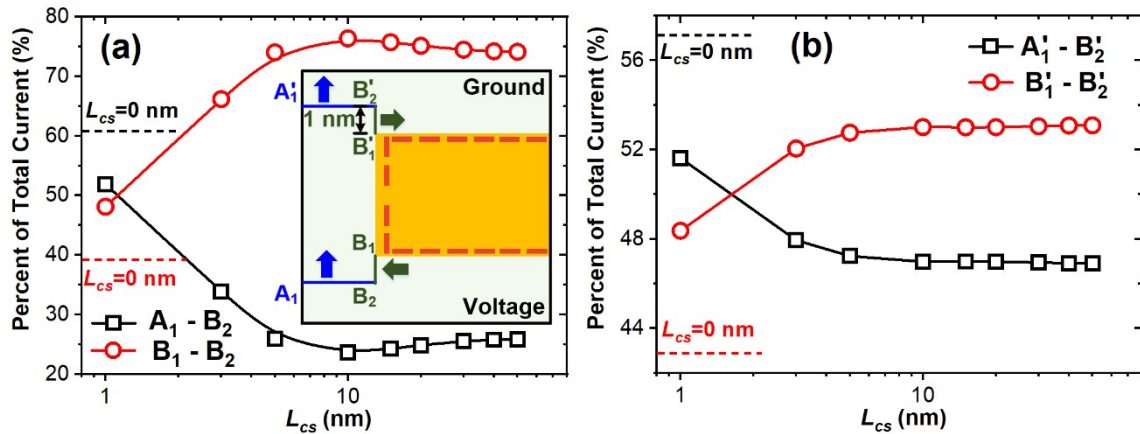


Figure S7. Percent of ionic current at different cross-sections at the entrance (a) and exit (b) of the nanopore. The inset shows the location of each cross-section. A₁-B₂

and A_1-B_2 are the cross-section locate at 1 nm away from the membrane. B_1-B_2 and $B_1'-B_2'$ are along the inner pore surface with a length of 1 nm.

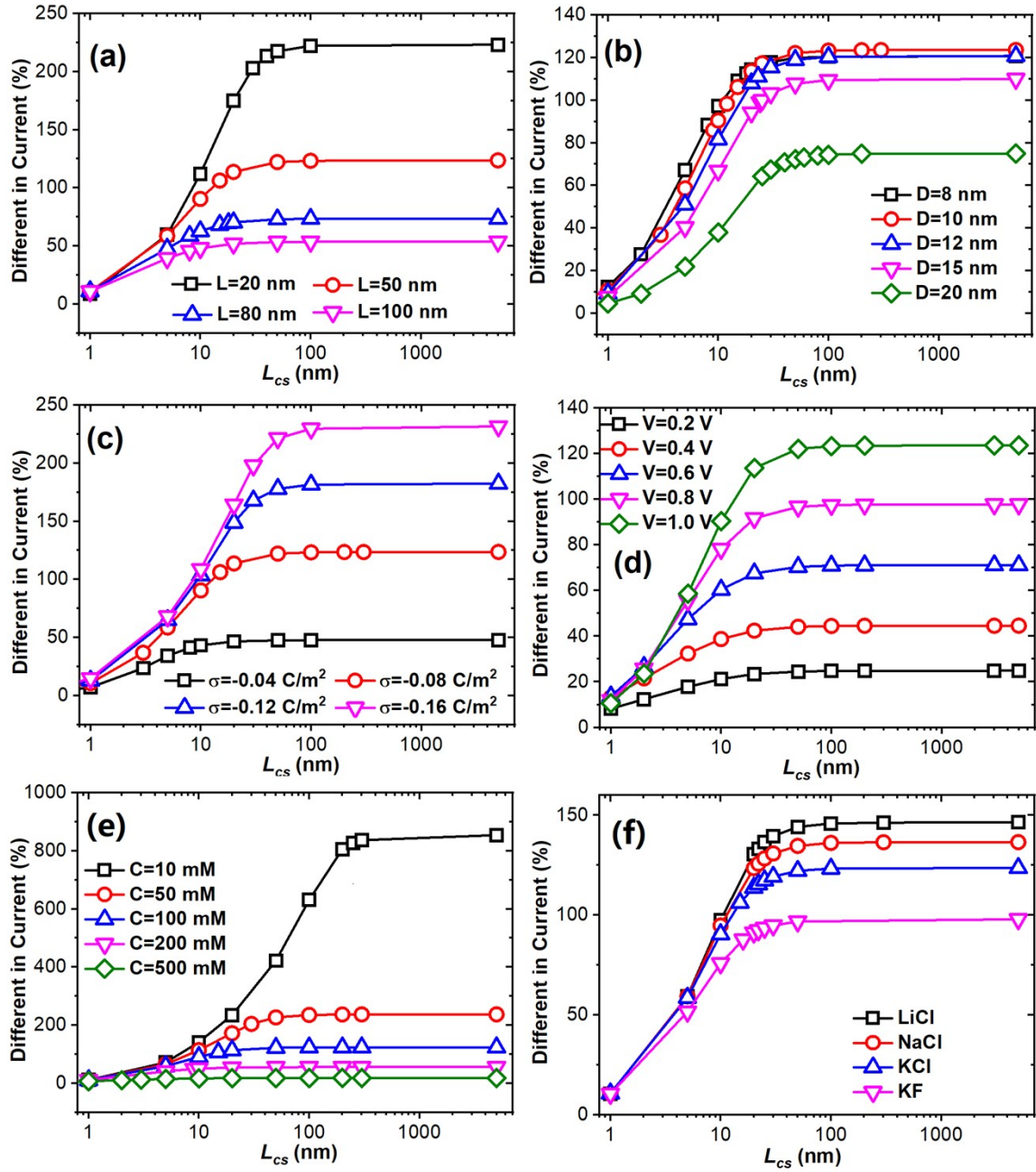


Figure S8. Enhancement of ionic current by the length (L_{cs}) of charged exterior surfaces under different conditions. (a) Pore length, (b) diameter, (c) surface charge density, (d) voltage, (e) salt concentration, and (f) salt type.

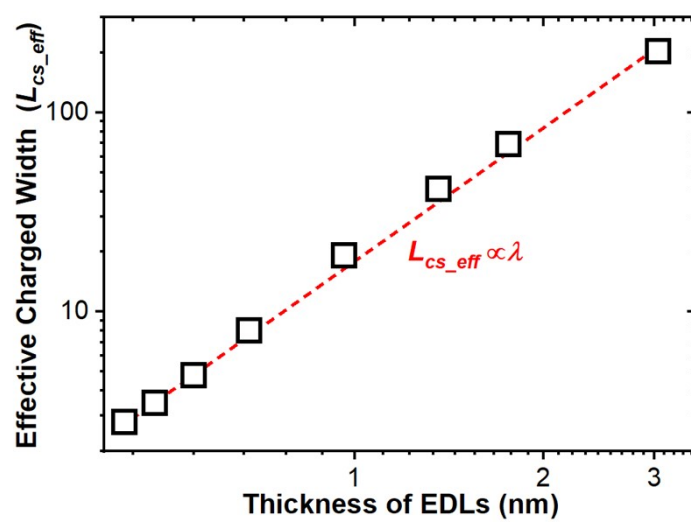


Figure S9. Effective charged length (L_{cs_eff}) under different thicknesses of EDLs.